Deterministic Approach for Multiple Source Tsunami Hazard Assessment for Sines, Portugal

M. Wronna[1,*] , R. Omira[1,3] , M. A. Baptista[1,2,3]

[1] Instituto Português do Mar e da Atmosfera, IPMA, I. P., Lisbon, Portugal

[2] Instituto Superior de Engenharia de Lisboa, Lisbon, Portugal

[3] Instituto Dom Luiz, University of Lisbon , IDL, Lisbon, Portugal

* Correspondence to: M. Wronna, IPMA, Rua C do Aeroporto, Lisbon, Portugal (martinwronna@gmail.com)

Abstract

In this paper, we present a deterministic approach for tsunami hazard assessment for the city and harbour of Sines - Portugal one of the test-sites of project ASTARTE. Sines holds one of the most important deep-water ports which contains oil-bearing, petrochemical, liquid bulk, coal and container terminals. The port and its industrial infrastructures are facing the ocean southwest towards the main seismogenic sources. This work considers two different seismic zones: the Southwest Iberian Margin and the Gloria Fault. Within these two regions, we selected a total of six scenarios to assess the tsunami impact at the test site. The tsunami simulations are computed using NSWING a Non-linear Shallow Water Model With Nested Grids. In this study, the static effect of tides is analysed for three different tidal stages MLLW (mean lower low water), MSL (mean sea level) and MHHW (mean higher high water). For each scenario, tsunami hazard is described by maximum values of wave height, flow depth, drawback, maximum inundation area and runup. Synthetic waveforms are computed at virtual tide gauges at specific locations outside and inside the harbour. The final results describe the impact at Sines test site considering the single scenarios at mean sea level, the aggregate scenario and the influence of the tide on the aggregate scenario. The results confirm the composite source of Horseshoe and Marques Pombal fault as the worst case scenario with wave heights above 10 m which reaching the coast approximately 22 minutes after the rupture. It governs the aggregate scenario with about 60% and inundates an area of 3.5 km².

Keywords: Tsunami hazard assessment, numerical modelling, aggregate scenarios

1 Introduction

Tsunamis are low frequency but high impact hazards for coastal societies. The December 26th, 2004 Indian Ocean and the March 11th, 2011 Tohoku striking tsunami events raised awareness due to the enormous loss of life and property. The Indian Ocean event in 2004 demonstrated the need for operational early warning systems around the world. However, seven years later, the 2011 Tohoku event showed the limitations of the scientific knowledge concerning tsunami sources, coastal impacts, and mitigation measures. Since then, in the NEAM region (North East Atlantic, Mediterranean and connected seas) many efforts have been addressed to understand better the tsunamigenic sources and to improve the tsunami hazard assessment capabilities. Within the NEAM region, the Gulf of Cadiz is among the most tsunami hazardous areas. The historical reports include events dated back to 60 BC (Mendonça, 1758, Baptista and Miranda, 2009; Kaabouben et al., 2009), but the geological evidence indicates high energy events back to 218 years BC (Luque et al., 2001).

The Portuguese coast is highly exposed to tsunami threat from local and regional active tectonic sources. The main tsunamigenic area is the SWIM (South West Iberia Margin), with a number of considerable SE dipping inverse faults (Fig. 2b) (Zitellini et al., 2009, Matias et al., 2013). The most severe tsunami was the 1st November, 1755 caused by the Lisbon earthquake with an estimated magnitude of 8.5 by Martins and Mendes Victor (1990). This magnitude was more recently re-evaluated by Solares and Arroyo (2004) with an estimate of 8.5±0.3. The tsunami hit the entire northern Atlantic basin with huge impact in Iberia and Morocco (Fig. 2) (Baptista and Miranda 2009). In the 20th century, the 28th February 1969 earthquake with a magnitude of 7.9 (Fukao, 1973) caused a small tsunami of 0.5 m amplitude in Lagos and Cascais (Fig. 1a) (Baptista et al., 1992; Baptista and Miranda, 2009). The tsunami waves hit the coast circa 3 a.m. (UTC) in low tide conditions (Baptista et al., 1992) but no significant damage was observed.

The second tsunamigenic zone to be considered is the Gloria Fault (Fig. 2c). The Gloria fault is a segment of the Eurasia-Nubia plate boundary. It is a large strike slip fault, located between 24ºW and 19ºW, with scarce seismic activity but was nonetheless the location of several large events during the 20th Century, in particular the 25th November 1941 earthquake, a submarine strike-slip event of magnitude 8.3-8.4 (Gutenberg and Richter, 1949) and the 26th May 1975 with magnitude 7.9 (Lynnes and Ruff, 1975; Grimson and Chen, 1986).

In recent years, a considerable number of tsunami hazard assessment studies were published for the North East Atlantic area. Most of these studies focus on the tsunami impact in the Gulf of Cadiz using a scenario based approach namely: Lima et al. (2010), Omira et al. (2010), Omira et al. (2011), Atillah et al. (2011), Baptista et al. (2011a), Renou et al. (2011), Omira et al. (2013), Benchekroun et al. (2013) and Lemos et al. (2014). Recently, Omira et al. (2015) published a probabilistic tsunami hazard assessment for the North East Atlantic.

In this study, we use a Deterministic Tsunami Hazard Assessment (DTHA) approach to evaluate the tsunami impact in Sines. The study area contains the country's most important deep water port which is connected to big industrial complexes by fragile infrastructure such as pipelines and conveyor belts. In summer the city is a popular tourist destination.

The DTHA approach consists of studying the impact of specific tsunami events – tsunami scenarios - in the study area. The impact is described in terms of maximum wave height (MWH), maximum flow depth (MFD), maximum drawback (MDB), maximum inundation area (MIA) and maximum inland penetration (MIP). We further built the aggregate scenario plotting the MWH and MFD in each cell considering the contribution of the individual scenarios (Tinti et al., 2011).

The final results are presented in integrated hazard maps for all the considered and the aggregate scenario. Each integrated hazard map consists of MWH, MFD, MDB, MIA and MIP of the corresponding scenario. The static effect of tides is analysed for three different tidal stages mean lower low water (MLLW), mean sea level (MSL), and mean higher high water (MHHW). Further we present the contribution of each scenario to the aggregate tsunami impact at MSL condition.

2 Study area and Digital elevation model

2.1 Study area

Sines is a city located on the west littoral margin of the Iberian Peninsula about 150 km south of Lisbon (Fig. 1a). The study area includes the city of Sines and parts of the surrounding municipality covering a coastline of about 35 km. The city has approximately 15000 inhabitants (Instituto Nacional de Estatística, 2011) and about 5000 floating population because of economic and touristic purpose.

Sines plays a major role in terms of energy production and storage. There are 2 great production centres of oil and gas industry (GALP refinery and Repsol YPF petrochemical industrial complex) which are connected via pipelines to oil-bearing and petrochemical terminal of Sines harbour (Câmara Municipal de Sines, 2007). The harbour is the country's most important deep water port (with 28 m depth) situated south of the city centre and consists of 5 terminals: liquid bulks, liquid natural gas, petrochemical, container and multipurpose; as well as fishing and leisure ports (Porto de Sines, 2014). The liquid natural gas terminal (LNG) contains facilities for loading and unloading processes of methane carriers, expedition facilities at LNG terminal depot, three LNG storage tanks, LNG processing facilities and natural gas dispatch facilities for the pipeline connecting the Sines LNG terminal to the Natural Gas Transport Network. At the multipurpose terminal coal is stored in stockpiles and is transported by a conveyor belt to Sines thermoelectric power plant. The power plant uses seawater for cooling of the generators which is captured and returned at the intake and restitution points close to São Torpes beach (Fig. 1b). The majority of the harbour facilities and big areas of the power plant are situated in possible inundation area below the 25 m topographic contour. The liquefied natural gas storage deposits is located right behind the port. In case of a destructive tsunami, facilities or leaking pipelines raise the danger of explosion and may cause an environmental disaster.

The study area limits are East to West from 8°47'00" to 8°55'00" and North to South from 37°58'00" to 37°55'00". In the northern part the landscape is designed by the influence of the magmatic batholith of Sines with a steep and rocky seafront. On the south westernmost part of the rocky outcrops begins the area of the port. The main jetty is facing south with a maximum elevation of 15 m above MSL and a width of 10 m (Fig. 1b). The liquid bulks terminal and petrochemical terminal are protected by the jetty against strong swell reaching the Portuguese coast mainly from northwest. The smaller jetties protect the fishing and leisure ports, which also protect the shell-shaped beach "Vasco da Gama" (Fig. 1b). Northwards is located the city centre and the majority of domestic property on the top of the batholith with altitudes higher than 25 m above sea level. Further east, the remaining terminals: multipurpose, container and natural gas protected by a recently enhanced jetty of approximately 2.5 km length (Fig. 1b). The container terminal is currently under construction due to expansion at the easternmost area of the port exposing new economic value to tsunami threat. Further southeast at the coast are situated the jetties to protect the intake and restitution points of the EDP thermoelectric power plant. Right beyond the jetties southwards begins the popular highly visited beach of "São Torpes" which is already a part of the natural park "Costa Vicentina" (Fig. 1b). The main port

areas and Vasco da Gama beach have their coastline facing southwards. The main tsunamigenic sources are located south of the study area. Due to its openness and exposure to the sea, the impact of tsunamis and other marine hazards like sea level rise are of great concern for the area.

2.2 Digital elevation model

In order to guarantee a good representation of the study area, we built a high-resolution Digital Elevation Model (DEM). We combined three different datasets and set them to the same reference system using GIS tools (Geographic Information System). We validated the final dataset using real time kinetic GPS on field trips. The DEM is crucial for computation of inundation on the dry land and near shore propagation.

Different types of datasets were used: a set of high resolution LIDAR dataset (Direção-Geral do Território, 2011), a bathymetric model (Instituto Hidrográfico de Portugal, 2012), and a nautical chart (Instituto Hidrográfico de Portugal, 2010). The LIDAR dataset of 2011 has a resolution of 2 m. The data is available in PT-TM06/ETRS89 projection and referenced to the altimetric datum of Cascais 2.08 m above hydrographic zero. The dataset of the bathymetric model contains a grid based point information 100 m spacing based on hydrographic surveys. In the overlapping areas of LIDAR dataset and the bathymetric model preference has been given to the more recent and higher resolution LIDAR dataset. For further improvement, the nautical chart of Sines (The nautical chart of Sines consists of 2 different charts one showing a more detailed view of the port with a scale of 1:12500 and the general chart of the test site with a scale of 1:30000) was scanned, geo-referenced, and digitized. Depth and altimetry data of the bathymetric model and the nautical charts are referenced to the hydrographic zero. All data was referenced to MSL which lays 2 m above hydrographic zero in Sines. In order to validate the final datasets we used field surveyed data points with GPS-RTK (Global Position System Real Time Kinetic). In order to fill gaps of the LIDAR data we used GPS-RTK to collect data to implement a recently constructed extension of a jetty not yet present in the datasets. After combination, validation and adaption of the existing datasets a grid representing the final study area with 10 m resolution has been computed. The resulting DEM properly represents Sines test site, especially the near shore areas, as LIDAR dataset is of very high resolution. The 10 m grid represents small rocky outcrops of the batholith in between Vasco da Gama beach and the leisure port. Other features like the connection to the main jetty in front of the multiuse-, liquid natural gas- and container-terminal or the jetty at the leisure port suffer from the low resolution.

3 Numerical Model and Nested Grids

Numerical modelling of tsunamis is commonly divided into three stages: generation, propagation, and inundation. We use an in-house developed and benchmarked numerical code NSWING (Non-linear Shallow Water Model with Nested Grids) (Miranda et al., 2014) to model the tsunami. The model supposes an instant seabed deformation that has been rendered using the half-space elastic theory (Okada, 1985) embedded in Mirone suite (Luis, 2007). The vertical sea bottom deformation is assumed to be equal to the free surface deformation and transferred to the ocean surface.

The code solves linear and non-linear approximations of shallow water equations (SWEs) to calculate tsunami propagation and inundation in a Cartesian or spherical reference system. In the deep ocean nonlinear convective inertia forces are of secondary order as waves travel with amplitudes much smaller than water depths. When the tsunami enters shallow coastal areas, the non-linear convective inertia force and bottom friction become increasingly important. We applied non-linear SWEs approximations in all instances, for deep-ocean, near-shore and on-shore propagation.

NSWING employs a dynamically coupled system of nested grids and solves SWEs using an explicit staggered finite leapfrog numerical scheme for linear terms and an upwind scheme for nonlinear terms. NSWING and the incorporation of the system coupled nested grids is mainly based on the code COMCOT (Liu et al., 1998). The code further applies a radiating boundary condition, allowing wave motion pass from one domain to other, through boundaries with very small reflections. A moving boundary algorithm (Liu et al., 1995), based on “wet” and “dry” cells, is adopted to track shoreline movement while inundation.

Propagation and behaviour of tsunamis change because of varying bathymetry when entering coastal areas. To model the impact in Sines we implement a dynamically coupled system of nested grids. We interpolated the half minute North Atlantic grid (GEBCO, 2014) to 640m resolution for the parent grid. Using four layers and applying a refinement factor of 4 we achieved 10m final resolution in the DEM.

The amplitude of the tide in south-west Portugal is above 2m and must be taken into account in Sines. (Baptista et al., 2011a) To study the tide effect, the tidal variation of the last three years have been considered. We used the values of Mean High Water (MHW) and Mean Low Water (MLW) from 2012 to 2014 and calculated the mean to obtain the MHHW and MLLW

respectively and referenced them to MSL.The MHHW is 1.22m above the MSL and the MLLW 0.88m underneath the MSL. These values have been subtracted and added respectively to the established DEM. For each designed scenario we ran the model in MHHW, MSL and MLLW conditions to study the static influence of the tide and is presented in the aggregate scenario (Antunes, 2014).

4 Tsunamigenic Scenarios

To design the tsunami scenarios we use the main seismogenic source zones and the associated Maximum Credible Earthquake (MCE) (Miranda et al., 2008; Omira et al., 2009). We used the typical faults (TFs) presented in Omira et al. (2009) except the Portimao Bank Fault (PBF) because it does not steer enough energy to the western Portuguese coast.

The seismogenic sources used here are SWIM and Gloria. For this study we considered four TFs in the SWIM area and their MCE scenarios to reproduce initial condition for tsunami propagation namely: the Cadiz Wedge Fault (CWF), the Gorringe Bank Fault (GBF), the Horseshoe Fault (HSF) and the Marques Pombal Fault (MPF) (Fig. 2b). Additionally we use a seismogenic scenario consisting of a composite rupture of HSF and MPF (HSMPF), proposed by Ribeiro et al. (2006) for the source of the 1st November 1755 earthquake. This source is also stated in Matias et al., (2013) with a maximum magnitude estimation of 8.75. This magnitude value coincides with the upper limit of the magnitude estimate for the 1755 earthquake of Solares and Arroyo (2004): 8.5±0.3. Once this source has been proposed we can not evaluate a worst case scenario impact without considering it.

The major tsunami event in the SWIM is the one associated with the 1st November 1755 earthquake and the exact source remains unknown. Numerous studies and campaigns have been carried out in order to solve the quest of the 1st November 1755 tsunamis source. Data (multi-channel reflection seismic, refraction seismic, multibeam swath Bathymetry) has been gathered to reveal more accurate information of the tectonic in the SWIM. This investigation in the SWIM area revealed numerous geological evidences of the used TFs. Several authors proposed distinct sources for this event.

Johnston (1996) suggested the GBF as a possible candidate source of the 1st November 1755 event through scale comparison of isoseismal maps with the 28th February 1969 event. Using tsunami backward ray tracing methods Baptista et al., (1998) suggested a source location for the 1755 tsunami closer to the Portuguese coast. Zitellini et al. (1999) found an active thrust

fault, the MPF through interpretation of multi-channel seismic data. Gutscher et al. (2002) concluded that the identified active subduction, the CWF is a candidate source for 1755 event and must be considered in natural hazard assessments. Further neotectonic structures and deformed seafloor sediments at the HSF also show clusters with shallow seismicity (Gràcia et al., 2003). Some authors suggest to consider multiple fault rupture scenarios to explain the high magnitude observed in 1755 (Zitellini et al., 2001, Gràcia et al., 2003, Ribeiro et al., 2006, Mendes-Victor et al., 2005). Nevertheless the exact source of the 1755 Lisbon event is still a matter of discussion. These uncertainties related to 1755 source and the tectonic processes acting in the SWIM confirm the need of systematic tsunami hazard assessment in surrounding areas.

The Gloria zone is our far field source area. The Gloria fault is a transform fault running from 24° West to 19° West (Laughton and Witmarsh, 1974). Three strong magnitude earthquakes occurred in the last 130 years: 22 December 1884 (Moreira, 1984), 25 November 1941 – Magnitude 8.3 (Gutenberg and Richter, 1949, Moreira, 1984) and 25 May 1975 – magnitude 7.9 (Lynnes and Ruff, 1975 and Grimson and Chen, 1986). The 25 November 1941 and the 26 May 1975 produced small tsunamis recorded in the tide stations in the North East Atlantic basin (Debrach, 1946, Moreira, 1984, Baptista et al., 1992, Baptista and Miranda, 2009). The 25 November 1941 epicenter location and the focal mechanism are presented in Baptista et al. (2011b). We used these parameters to draw a 1941 like scenario for the Gloria source zone. The TF parameters are presented in table 1 and the fault is presented in figure 2.

5 Results

We ran a total of eighteen simulations. For each typical fault we considered three tide conditions: Mean Lower Low Water (MLLW), Mean Sea Level (MSL) and Mean Higher High Water (MHHW). The results are presented in integrated maps of maximum wave height (MWH), maximum flow depth (MFD), maximum drawback (MDB), maximum inundation area (MIA) and maximum inland penetration (MIP) (Fig. 3a-e). For the scenarios at MSL, we additionally present synthetic waveforms (Fig. 4 and 5) at chosen positions (Fig. 1b).

In figure 6 we present the aggregate scenario considering all calculated models. Figure 7 shows the inundation and the drawback limits considering the aggregate scenarios at the three tide conditions.

5.1 MSL Results

The analysis of figures 3 - 5 shows that all SWIM scenarios produce heavier inundation and drawback in comparison to the Gloria fault scenario. The Gloria scenario produces MWH values of approximately 1m while the SWIM scenarios produce MWH above 10 m. Figures 3 - 5 present results of the individual scenarios and their absolute values are summarized in table 2. The HSMPF scenario, corresponding to the worst case scenario, produces 18.6 m of MWH and 3.47 km² of inundated area. Detailed analysis of figure 3d shows flow depths greater than 0.5 m in 90% of the inundation area. The GBF and HSF scenarios, with MWH above 15 m, also produce inundation above 3 km² (cf. table 2 and Fig. 3b and Fig. 3c). The remaining SWIM scenarios (CWF and MPF) still produce MWH above 10 m and leave more than 2 km² inundated.

Among the SWIM scenarios, the MPF produces the weakest impact in Sines but still with MWH above 10 m (cf. Fig. 3e). Maximum runup up to 19.3 m occurs during the HSF scenario at the south of the test site (cf. table 2). All SWIM scenarios produce sufficient drawback (see blue lines in figure 3a-e) to leave the intake and restitution points of the thermoelectric power plant dry. MDB occurs during the composite tsunami model HSMPF. The Gloria scenario produces 1.2 m MWH in certain areas and inundates low lying areas such as beaches. The flooded area of the Gloria scenario is less than 0.2 km² and the area at the intake and restitution points does not stay dry (Fig. 5a and table 2).

The analysis of the synthetic waveforms at the virtual stations shows similar periods and tsunami travel time (Fig. 4) for all SWIM scenarios. First arrival occurs in all records at point P3 (blue curves in figure 4 and figure 5b). Clearly distinguishable are the records for the Gloria scenario presented in figure 5b which shows an arrival time of about 85 minutes after initial sea surface displacement. The maximum amplitude is about 0.4 m with a period of approximately 10 minutes (Fig. 5b). The record in tide gauge point P2, at 5.6 m depth right in front of the intake and restitution points, confirms that no considerable drawback is happening throughout the event (Fig. 5b). The records of the SWIM scenarios GBF, HSF, HSMPF, MPF show periods of 15 to 20 minutes and for the CWF approximately 25 minutes. Maximum amplitudes are obtained at the tide gauge P2 for the tsunamis produced by CWF at the 3rd wave, HSF and HSMPF at the 1st and 3rd wave, respectively. At point P2 waveforms indicate that the cell stays at least once dry for all SWIM scenarios (Fig. 4). Attenuation is visible for all scenarios after 6 hours runtime except for the Gloria scenario where attenuation occurs after 15 hours.

5.2 The aggregate scenario and the influence of the tide

The aggregate scenario map depicts the extreme hazard values field point by taking the envelope of all individual scenarios. We present aggregate scenarios of MWH, MFD, MDB, MIA and MIP for the different tide conditions (Fig. 6).

The aggregate scenario map (Fig. 6), considering all stages of the tide, shows 4.8 km² MDB area and 4.1 km² maximum inundated area. Maximum runup values over 20 m occur close to the cliffs at Vasco da Gama beach and are reached in MHHW condition. In other areas, such as behind the liquid bulks and petrochemical terminal and at the railway connection to the port, maximum runup values exceed 15 m. MWHs above 10 m have been modelled along the entire coastline (Fig. 6). In high tide condition the inundation area is over 4 km² and 3.5 km² in low tide condition considering the aggregate scenario. Inundation area is 5% bigger at MSL and 14% at MHHW compared to MLLW (Fig. 7). MDB area is 16% greater at MLLW and 11% greater at MSL than in MHHW conditions (Fig. 7). The flooded area at Vasco da Gama beach is not significantly bigger at MHHW as the area behind the beach is confined by the steep topography. Moreover figure 6 shows that the mean MFD values are about 1.5 m higher at MHHW than at MLLW in the area of the beach. Other areas behind the multipurpose and container terminal or at São Torpes beach show clearly greater inundation areas in high tide condition (Fig. 7). The limits of MDB and MIP for the aggregate scenario concerning MLLW, MSL and MHHW are mapped in figure 7.

6 Discussion and Conclusions

We ran a total of 18 scenarios to study the tsunami impact at Sines. Our results show that all SWIM scenarios cause severe inundation and drawback. To complement the integrated hazard maps of MWH, MFD, MDB, MIA and MIP we recorded synthetic waveforms at chosen points (see figure 1). The signals of the waveforms are diverse. This fact may be explained due to differences in the TF parameters. Waveforms from HSF, MPF, GBF and HSMPF are comparable in terms of period and arrival time (Fig. 4a-e). These TFs are dextral reverse with SW-NE trending and the hanging block in the SE. They are all located in the SWIM area. They are distinguishable through their dimensions and slip. Other parameters like strike, dip and rake are similar. Among the single fault scenarios the GBF is the biggest single fault producing 17.1 m MWH in the study area (see table 2). The HSF, although smaller, produces a similar inundation and wave height pattern as the slip is 5 m higher compared to the GBF (see table 1).

The MPF is smaller in terms of dimensions and has a slip of 8 m and therefore produces the weakest tsunami in the SWIM (Table 1 and Fig. 3e). Nevertheless, MWHs are above 10 m and MPF is the nearest fault to the test site that produces short tsunami travel time (22 minutes in figure 4e). The composite scenario HSMPF is the worst case scenario and combines the effects of both faults: First wave arrives 22 min after the earthquake and tsunami triggered by HSMPF causes worst inundation and drawback in Sines. The CWF is a subduction slab and has different fault parameters compared to the other TFs in the SWIM. The shallow east dipping slab has dimensions of 170x200 km and a slip of 20 m (see table 1). The analysis of the waveforms shows that wave periods generated by the CWF are larger than the others from the TFs in the SWIM. This fact may be explained by the larger displaced area by this scenario. Cape St. Vincent (Fig. 2b) in the southwest of Portugal might act as an obstacle to the tsunami leading to reduce the impact. The CWF has higher impact in the southern part of the study area but with decreasing inundation and amplitudes towards the north. Nevertheless, wave amplitudes of 5 m cause considerable inundation in the northern part of the port. The waves produced by CWF reach Sines 38 minutes after the earthquake (Table 2). The Gloria fault located at 37°N between 14°W and 24°W produces the smallest inundation in the study area. It is a transform fault triggering slight vertical movement because of 160° rake with a slip of 11 m (Table 2). The scenario produces amplitudes between 0.3 - 0.4 m with approximately 10 minute period (Fig. 5b). The earthquake in 1941 generated similar waveforms showing weak attenuation with amplitudes around 0.4 m in Cascais (Baptista et al., 1992; Baptista and Miranda, 2009). Site effects, observed in some few coastal locations (Fig. 5a), caused MWH over 1 m with some smaller inundation in unhabituated area between the container terminal and the intake and restitution points of the EDP power plant. Because of the larger distance to the Portuguese coast the tsunami travel time is approximately 85 minutes (Table 2).

We also calculated flow velocities for the composite scenario HSMPF at MSL for different stages of tsunami propagation. The median values are about 10 m/s in the inundation area at all terminals in the port. Some extremes of about 20 m/s or higher occur close to the jetties and in the inundation area when the flow depth values are small depending on the considered propagation instant. In general we find that flow velocities increase with lower flow depth values in the inundation area.

Considering the HSMPF scenario in MSL conditions the pipelines at the liquid bulk and petrochemical terminal are entirely inundated with up to 5 m flow depth values. These structures are subject to flow velocities of about 10 m/s at first wave impact. At the 17 m

topographic contour, the pipelines behind the liquid bulk and petrochemical terminal are not affected by the tsunami (Fig 3d). We find similar flow velocity values at the multipurpose terminal where the pipelines of the liquefied natural gas storage tanks pass. Here the maximum flow velocity values there are slightly above 10 m/s at wave impact, and MFD are between 5 – 10 m. The conveyor belt and the stockpiles at the multipurpose are nearly entirely inundated up to 5 m and show flow velocities of 10 m/s at first wave impact. The pipelines at the liquid bulk, petrochemical and multipurpose terminal are inundated by all scenarios in the SWIM. These quantitative DTHA results indicate a high risk of potential damage in case of tsunami impact. However, in the building vulnerability is beyond the scope of this study.

The tide has important influence on tsunami impact in Sines. The tidal regime is semi-diurnal with an amplitude of about 2 m. As expected the aggregate scenario at MHHW condition caused larger inundation areas and higher MFD values. On the other hand the aggregate scenario at MLLW produced larger drawback areas. A tsunami impact at low tide does not exclude the risk of heavy inundation and increases MDB by 16% compared to MHHW (Fig. 7).

Our results are compatible with the PTHA results for the Northeast Atlantic. Omira et al. (2015) show that wave heights exceeding 5 m have a probability of 45% of occurrence in 500 years at Sines. Only the scenarios of the SWIM area have the capacity to produce such high tsunami impact along the Portuguese west shore. Moreover our results are comparable with the unique historical report showing that the tsunami did not reach the city (Falcão, 1987).

We computed a map showing the contribution of the individual scenarios to the aggregated scenario at MSL (Fig. 8). Four scenarios contribute to the aggregate scenario, namely CWF, GBF, HSF and HSMPF. The main actor in the aggregated model is the HSMPF scenario that contributes with more than 60% independent of the tidal amplitude (Table 3). The scenarios CWF, GBF, HSF contribute about 12±4% to the aggregate model. The MPF and Gloria do not contribute to the aggregate scenario (Table 3 and Fig. 8).

Concluding we find that all SWIM scenarios (CWF, GBF, HSF, MPF and HSMPF) demonstrate high impact in Sines test site. Still the weakest source, the MPF, causes considerable inundation and MWH above 10 m. The proximity of the faults within the SWIM results in short tsunami travel times. For the models MPF and HSMPF we calculated 22 minutes propagation time from the source to Sines test site. This closeness to possible tsunami sources raises the need of an efficient early warning system and meticulously planned evacuation for the port and other

coastal areas. Also, coastal societies need to be educated and prepared for possible tsunami impact.

The Gloria fault differs from the other scenarios and produces MWH of approximately 1 m in certain areas, one order of magnitude less than the scenarios in the SWIM.

The aggregate scenario allows to consider a set of faults to produce a synthesis of different scenarios. We further state the importance of this tool as important indicator for evacuation and city planners. We showed with the contribution map that different sources play varying importance in our study area. Although the worst case scenario may contribute more to the aggregate scenario than other considered faults, still other faults may have more significant impact on other parts of the test-site. The aggregate scenario is a valuable tool for quantitative presentation of tsunami impact from multiple sources. Especially in areas exposed to threat from near-field sources, the aggregate scenario maps help establishing accurate evacuation plans and thus allowing efficient and faster reaction to tsunami warning.

Acknowledgements

This work is funded by ASTARTE - Assessment, Strategy And Risk Reduction for Tsunamis in Europe - FP7- ENV2013 6.4-3, Grant 603839. The authors wish to thank Commandant José Brazuna Fontes of Sines harbour for his support for the field survey and Direção Geral do Território for making available LIDAR data of the study area. Finally, the authors wish to thank the reviewers for their suggestions that greatly improved the paper.

References

Antunes C.: Tabelas de Máximos, Médias e Mínimos. [online] Available at: <http://webpages.fc.ul.pt/~cmantunes/hidrografia/hidro_tabelas.html> [accessed 18th November 2014], 2014.

Atillah, A., El Hadani, D., Moudni, H., Lesne, O., Renou, C., Mangin, A. and Rouffi, F.: Tsunami vulnerability and damage assessment in the coastal area of Rabat and Salé, Morocco. Natural Hazards and Earth System Sciences, 11, 3397-3414., 2011.

Baptista, M. A., Miranda, P. and Victor, L. M.: Maximum entropy analysis of Portuguese tsunami data; the tsunamis of 28.02. 1969 and 26.05. 1975. Sci. Tsunami Hazards, 10(1), 9-20, 1992.

Baptista, M. A., Miranda, P. M. A., Miranda, J. M. and Victor, L. M.: Constrains on the source of the 1755 Lisbon tsunami inferred from numerical modelling of historical data on the source of the 1755 Lisbon tsunami. *Journal of Geodynamics*, *25*(1), 159-174, 1998.

Baptista, M. A. and Miranda, J. M.: Revision of the Portuguese catalog of tsunamis. Natural Hazards and Earth System Science, 9(1), 25-42, 2009.

Baptista, M. A., Miranda, J. M., Omira, R. and Antunes, C.: Potential inundation of Lisbon downtown by a 1755-like tsunami. Natural Hazards and Earth System Science, 11(12), 3319-3326, 2011a.

Baptista, M. A., Miranda, J. M., Batllo, J. and Macia, R.: North East Atlantic Tsunamis Related with Gloria Fault. AGU Fall Meeting Abstracts, Vol. 1, p. 1530, 2011b.

Benchekroun, S., Omira, R., Baptista, M. A., El Mouraouah, A., Brahim, A. I. and Toto, E. A.: Tsunami impact and vulnerability in the harbour area of Tangier, Morocco. Geomatics, Natural Hazards and Risk, doi:10.1080/19475705.2013.858373, 2013.

Câmara Municipal de Sines: Munícipio de Sines. [online] Available at: <http://www.sines.pt/PT/Negocios/potencialidades/turismo/Paginas/default.aspx> [accesssed 18th September 2014], 2007 (in Portuguese)

Debrach, J. Raz de marée d'origine sismique eneregistrée sur le litoral Atlantique du Maroc, Service de Physique du Globe et de Meteorologie, Annales. Maroc ,1946.

Direção-geral do Território: Modelo Digital do Terreno das Zonas Costeiras de Portugal Continental com resolução de 2 m (600 m mar, 400 m terra) – LiDAR. Direção de Serviços de

Geodesia e Informação Geográfica. Direção-Geral do Território (DGT). Metadata ID: 75d36fe737e241d3ac29c42ba7114403. 2011.

Falcão, J., A.: Memória paroquial do Concelho de Sines em 1758. Santiago do Cacém : Real Soc.Arq.Lusitana, 1987.

Fukao, Y.: Thrust faulting at a lithospheric plate boundary the Portugal earthquake of 1969. *Earth and Planetary Science Letters*, *18*(2), 205-216, 1973.

GEBCO: The General Bathymetric Chart of the Oceans, GEBCO_2014 Grid, version 20150318. [online] Available at: <http://www.gebco.net> [accessed July 2014], 2014.

Gràcia, E., Dañobeitia, J., Vergés, J., and PARSIFAL Team.: Mapping active faults offshore Portugal (36 N–38 N): implications for seismic hazard assessment along the southwest Iberian margin. *Geology*, *31*(1), 83-86, 2003.

Grimison, N. L. and Chen, W. P.: The Azores-Gibraltar plate boundary: Focal mechanisms, depths of earthquakes, and their tectonic implications. Journal of Geophysical Research: Solid Earth (1978–2012), 91(B2), 2029-2047, 1986.

Gutenberg, B. and Richter, C. F.: Seismicity of the Earth and associated phenomena. Princeton University Press, Princeton, New Jersey, 1949.

Gutscher, M. A., Malod, J., Rehault, J. P., Contrucci, I., Klingelhoefer, F., Mendes-Victor, L., and Spakman, W.: Evidence for active subduction beneath Gibraltar. *Geology*, *30*(12), 1071-1074, 2002.

Instituto Hidrográfico de Portugal: Aproximações a Sines. Plano de Porto de Sines n° 26408. 3rd Edition. Marinha, Instituto Hidrográfico. Lisbon, 2010.

Instituto Hidrográfico de Portugal: Bathymetric Model of Sines. Modelo Batimetrico de Sines. [online] Available at: <http://www.hidrografico.pt/download-gratuito.php> [accessed 4th April 2014], 2012.

Instituto Nacional de Estatística: Census 2011. [online] Available at: <http://censos.ine.pt/xportal/xmain?xpid=CENSOS&xpgid=censos2011_apresentacao> [accessed 18th September 2014], 2011.

Johnston, A. C.: Seismic moment assessment of earthquakes in stable continental regions—III. New Madrid 1811–1812, Charleston 1886 and Lisbon 1755. *Geophysical Journal International*, *126*(2), 314-344, 1996.

Kaabouben, F., Baptista, M. A., Iben Brahim, A., Mouraouah, A. E. and Toto, A.: On the moroccan tsunami catalogue. *Natural Hazards and Earth System Science*, *9*(4), 1227-1236, 2009.

Laughton, A. S. and Whitmarsh, R. B.: The Azores-Gibraltar plate boundary. In Geodynamics of Iceland and the North Atlantic area, *NATO Advanced Study* Institute, *Reykjavik*, Springer Netherlands, 63-81, 1974.

Lemos, C. R., Omira, R., Pinheiro, L. M., Baptista, M. A., Quaresma, L. S. And Garrido, C.: Tsunami Impact from a 1755-like event in the Aveiro Region, Portugal. In *EGU General Assembly Conference Abstracts* (Vol. 16, p. 15629), 2014.

Lima, V. V., Miranda, J. M., Baptista, M. A., Catalão, J., González Rodríguez, E. M., Otero, L. ... and Carreño Herrero, E.: Impact of a 1755-like tsunami in Huelva, Spain, Nat. Hazards Earth Syst. Sci., 10, 139–148, 2010.

Liu, P. L. F., Cho, Y. S., Briggs, M. J., Kanoglu, U. and Synolakis, C. E.: Runup of solitary waves on a circular island. *Journal of Fluid Mechanics*, *302*, 259-285, 1995.

Liu, P. L., Woo, S. B., and Cho, Y. S.: Computer programs for tsunami propagation and inundation. *Cornell University*, 1998.

Luis, J. F.: Mirone: A multi-purpose tool for exploring grid data. *Computers & Geosciences*, *33*(1), 31-41, 2007.

Luque, L., Lario, J., Zazo, C., Goy, J. L., Dabrio, C. J. and Silva, P. G.: Tsunami deposits as paleoseismic indicators: examples from the Spanish coast. *Acta geológica hispánica*, *36*(3), 197-211, 2001.

Lynnes, C. S. and Ruff, L. J.: Source process and tectonic implications of the great 1975 North Atlantic earthquake. *Geophysical Journal International*, *82*(3), 497-510, 1985.

Martins, I., and Mendes-Víctor, L. A.: *Contribuição para o estudo da sismicidade de Portugal Continental*. Universidade de Lisboa, Instituto Geofísico do Infante D. Luís, Edição 18 de Publicação, 1990.

Matias, L. M., Cunha, T., Annunziato, A., Baptista, M. A., and Carrilho, F.: Tsunamigenic earthquakes in the Gulf of Cadiz: fault model and recurrence. *Natural Hazards and Earth System Science*, *13*(1), 1-13, 2013.

Mendonça, J. M.: História Universal dos Terramotos que tem havido no mundo desde que ha noticia, desde a sua criação até ao século presente. *Arq Nac da Torre de Tombo, Lisboa–Portugal*, 1758.

Miranda, J. M., Baptista, M. A., Terrinha, P. and Matias, L.: Tsunamigenic source areas for Portugal mainland, Iberia, Oral Communication, Session on Tsunami Early Warning Systems and Tsunami Risk Mitigation in the European-Mediterranean Region, 31st General Assembly of the European Seismological Commission, Crete, Greece, 2008.

Miranda, J. M., Luis, J. F., Reis, C., Omira, R., and Baptista, M. A.: Validation of NSWING, a multi-core finite difference code for tsunami propagation and run-up, American Geophysical Union (AGU) Fall Meeting, San Francisco. Paper Number : S21A-4390. Session Number and Title: S21A, Natural Hazards, 2014.

Okada, Y.: Surface deformation due to shear and tensile faults in a half-space. *Bulletin of the seismological society of America*, *75*(4), 1135-1154, 1985.

Omira R., Baptista M. A., Matias L., Miranda J. M., Catita C., Carrilho F., and Toto E.: Design of a Sea-level Tsunami Detection Network for the Gulf of Cadiz. Nat *Natural Hazards and earth System Science*, 9:1327-1338, 2009.

Omira, R., Baptista, M. A., Miranda, J. M., Toto, E., Catita, C. and Catalao, J.: Tsunami vulnerability assessment of Casablanca-Morocco using numerical modelling and GIS tools. *Natural hazards*, *54*(1), 75-95, 2010.

Omira, R., Baptista, M. A. and Miranda, J. M.: Evaluating tsunami impact on the Gulf of Cadiz coast (Northeast Atlantic). *Pure and applied geophysics*, *168*(6-7), 1033-1043, 2011.

Omira, R., Baptista, M. A., Leone, F., Matias, L., Mellas, S., Zourarah, B. ... and Cherel, J. P.: Performance of coastal sea-defense infrastructure at El Jadida (Morocco) against tsunami threat: lessons learned from the Japanese 11 March 2011 tsunami. *Natural Hazards and Earth System Sciences*, *13*, 1779-1794, 2013.

Omira, R., Baptista, M. A. and Matias, L.: Probabilistic Tsunami Hazard in the North East Atlantic from Near- and Far-field Tectonic Source. Pure App. Geophys., 172(3-4): 901-920, 2015.

Porto de Sines: Administração dos portos de Sines e do Algarve S.A. [online] Available at: < http://www.portodesines.pt/> [accessed 18th September 2014], 2014.

Renou, C., Lesne, O., Mangin, A., Rouffi, F., Atillah, A., El Hadani, D. and Moudni, H.: Tsunami hazard assessment in the coastal area of Rabat and Salé, Morocco. *Natural Hazards and Earth System Sciences*, *11*, 2181-2191, 2011.

Ribeiro, A., Mendes-Victor, L., Cabral, J. M. L. C., Matias, L., and Terrinha, P.: The 1755 Lisbon earthquake and the beginning of closure of the Atlantic. European Review, 14(02), 193-205, 2006.

Solares, J. M., and Arroyo, A. L.: The great historical 1755 earthquake. Effects and damage in Spain. *Journal of Seismology*, *8*(2), 275-294, 2004.

Tinti, S., Tonini, R., Bressan, L., Armigliato, A., Gardi, A., Guillande, R. ... and Scheer, S.: Handbook of tsunami hazard and damage scenarios. *JRC scientific and technical reports*. EUR 24691 EN, JRC61463, Luxembourg (Luxembourg), OP, doi:10.2788/21259, 2011.

Zitellini, N., Chierici, F., Sartori, R. and Torelli, L.: The tectonic source of the 1755 Lisbon earthquake and tsunami, Ann. Geofis., 42, 49–55, 1999.

Zitellini, N., Mendes, L. A., Cordoba, D., Danobeitia, J., Nicolich, R., Pellis, G. ... and Ruiz, A. Z.: Source of 1755 Lisbon earthquake and tsunami investigated. *Eos, Transactions American Geophysical Union*, *82*(26), 285-291, 2001.

Zitellini, N., Gràcia, E., Matias, L., Terrinha, P., Abreu, M. A., DeAlteriis, G. ... and Diez, S.: The quest for the Africa–Eurasia plate boundary west of the Strait of Gibraltar. *Earth and Planetary Science Letters*, *280*(1), 13-50, 2009.

Table 1. Fault parameters of the tsunamigenic sources considered in this study. These parameters have been used for the 3 cases of the tide MHHW, MSL and MLLW.

Fault	L [km]	W[km]	Rake [°]	Strike [°]	Dip [°]	Slip [m]	Depth [km]	μ [Pa]	Mw
HSF	165	70	90	42.1	35	15	5	4.5e+10	8.5
MPF	110	70	90	20.1	35	8	5	4.5e+10	8.25
CWF	170	200	90	349	5	20	5	3.0e+10	8.75
GBF	200	80	90	53	35	10	5	4.5e+10	8.5
HSM PF	165/110	70/70	90/90	42.1/20.1	35/35	15/8	5/5	4.5e+10/ 4.5e+10	8.75
Gloria	200	50	160	82	88	11	1	3.0e+10	8.3

Table 2. Synthesis of the Results: MFD, MWH, MIA, MDB area, maximum runup and arrival time for all scenarios at MSL.

Scenario (MSL)	MFD [m]	MWH [m]	MIA [km²]	MDB area [km²]	Maximum runup [m]	Arrival Time [min]
CWF	12.2	12.8	2.71	2.98	14.1	38
HSF	13.3	15.7	3.16	3.37	19.3	30
GBF	12.4	17.1	3.18	3.02	18.9	25
HSMPF	13.1	18.6	3.47	3.80	17.5	22
MPF	9.1	10.7	2.07	1.98	11.3	22
Gloria	0.9	1.2	0.19	0.22	4.3	85

Table 3. Contribution of the scenarios considering MWH and MFD to the aggregate model at the 3 stages of the tide.

Scenario	CWF [%]	GBF [%]	HSF [%]	HSMPF [%]
AGG MHHW	8.3	15.8	9.9	66
AGG MSL	15.1	12.4	10.0	62.5
AGG MLLW	16.8	11.7	11.1	60.3

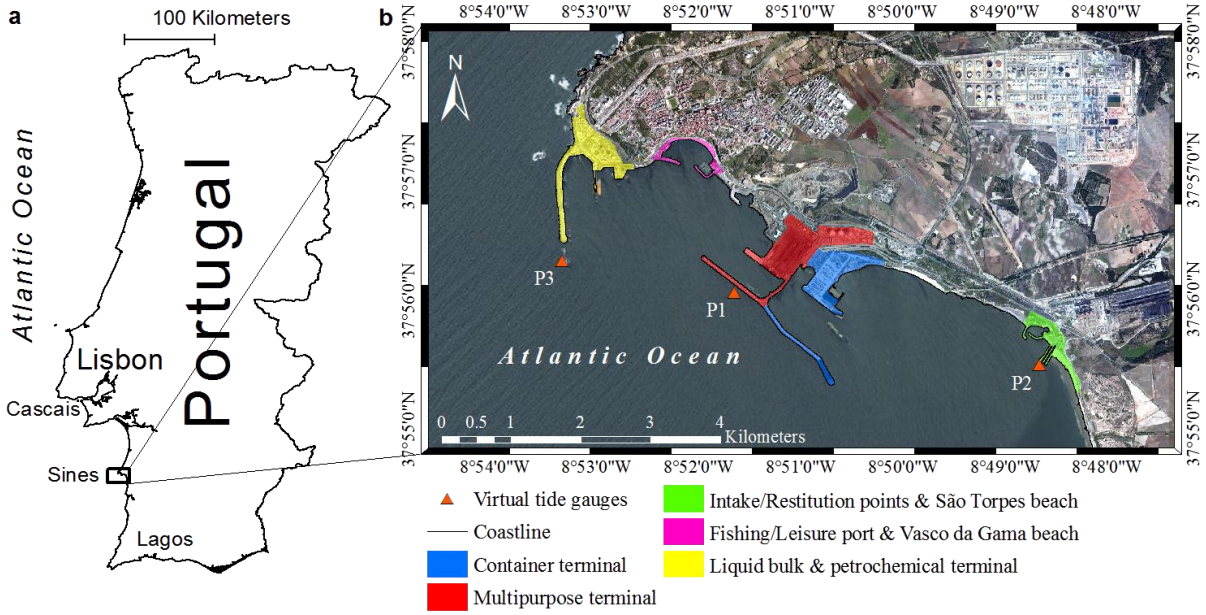

1

2

3 Figure 1. (a) General map: Location of Sines test site; (b) test site map identifying general
4 features and tide gauges for synthetic wave forms.

5

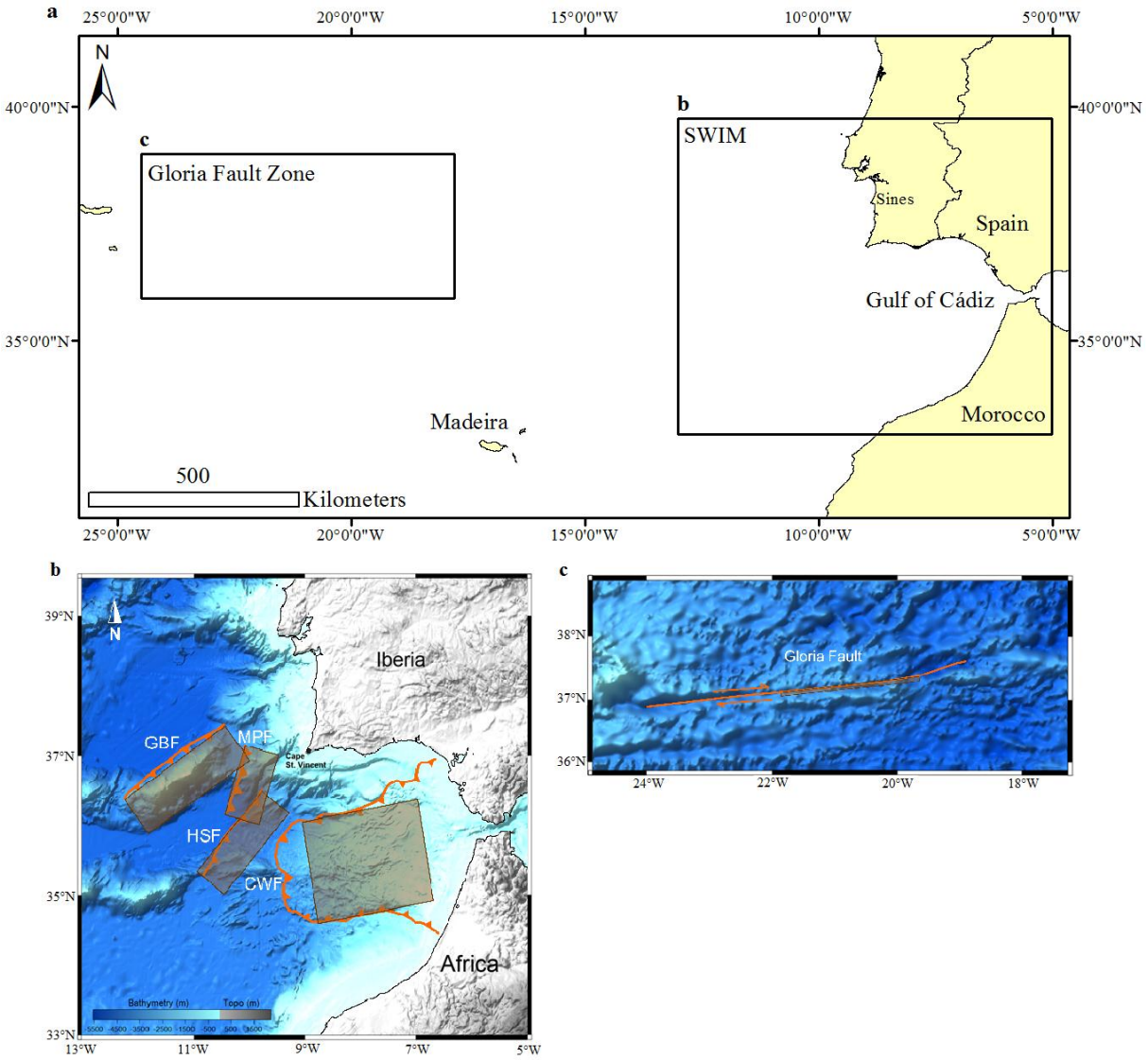

Figure 2. (a) Location of the Source Zones; (b) TFs used for Tsunami modeling in the SWIM. Dextral reverse faults: Gorringe Bank fault (GBF), Marques Pombal fault (MPF), Horseshoe fault (HSF); Subduction slab: Cadiz Wedge Fault (CWF); (c) Dimension and geographic location of the Gloria fault (red line) considered in this study. The grey rectangles indicate the fault planes used for modelling.

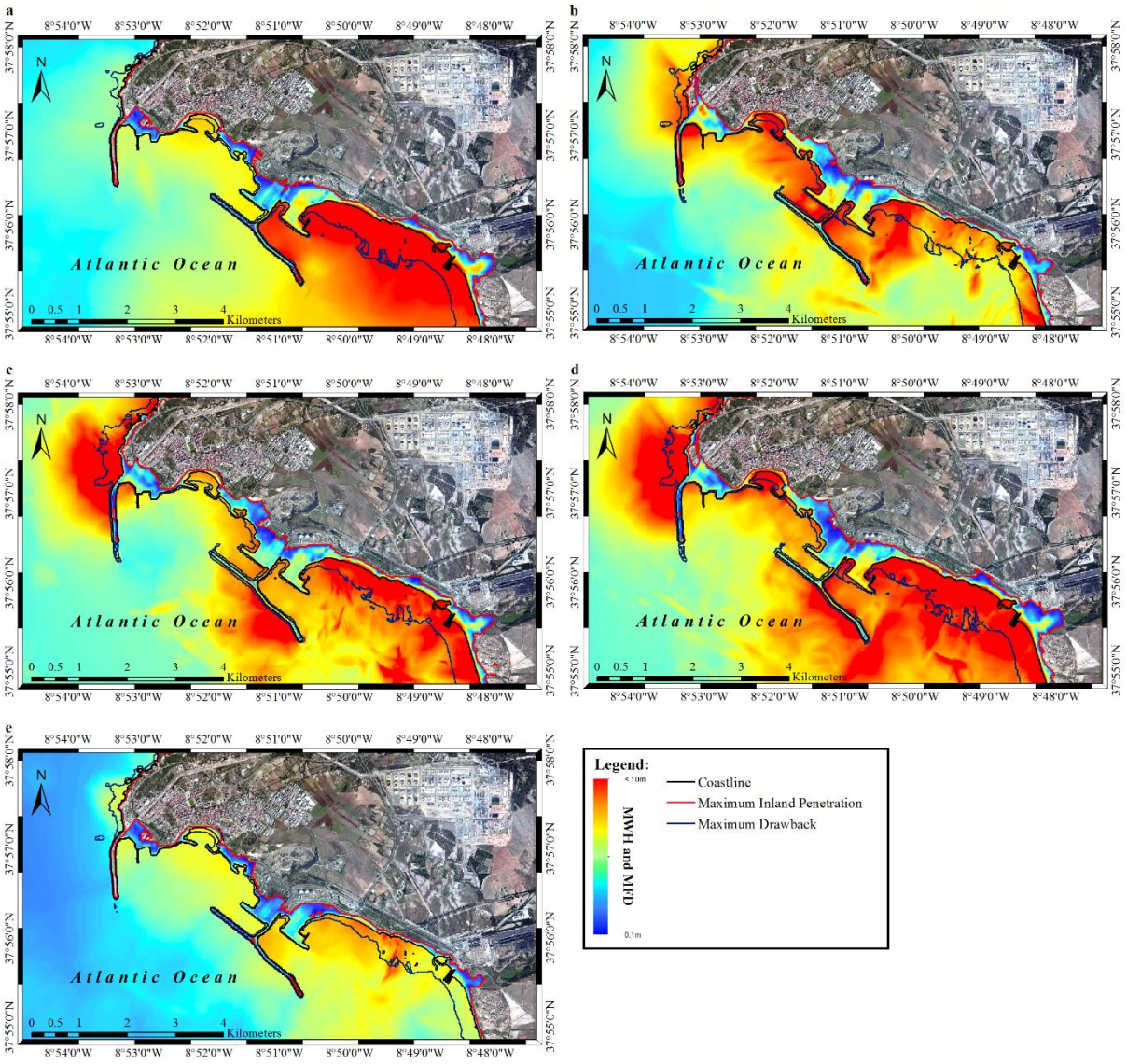

Figure 3. Results of MWH, MFD, MDB, MIA and MIP of the SWIM scenarios considering MSL: (a) CWF, (b) GBF, (c) HSF, (d) HSMPF, (e) MPF. MWH and MFD are presented by the colour bar in the lower right corner offshore and on land respectively. Offshore and land are separated by the coastline (black line). MDB is indicated by the dark blue line. The MIA is given between the coastline and the MIP (red line).

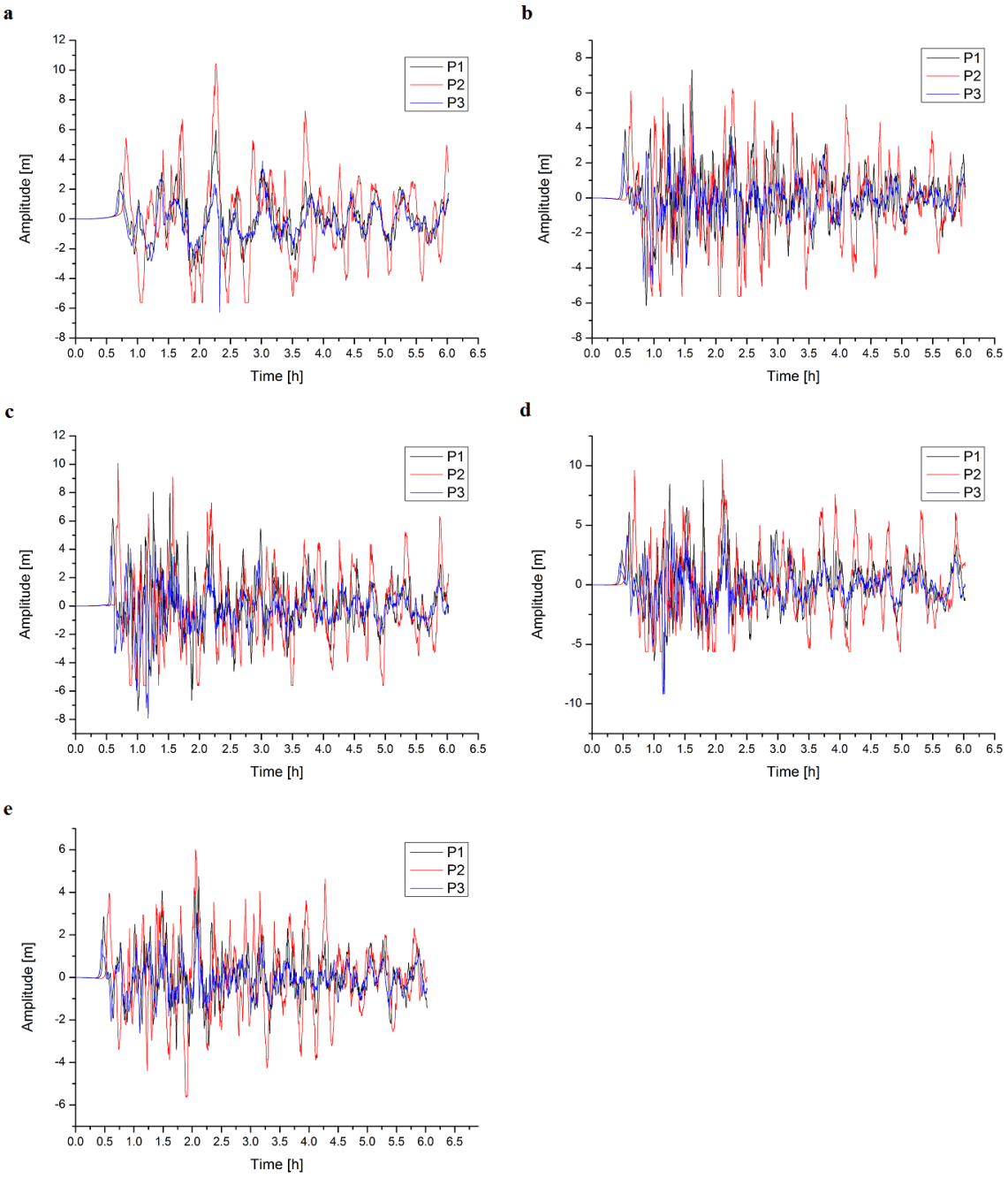

Figure 4. Synthetic waveforms for 6h propagation time at 3 chosen points (cf. Fig. 1) for the SWIM scenarios: (a) CWF, (b) GBF, (c) HSF, (d) HSMPF, (e) MPF.

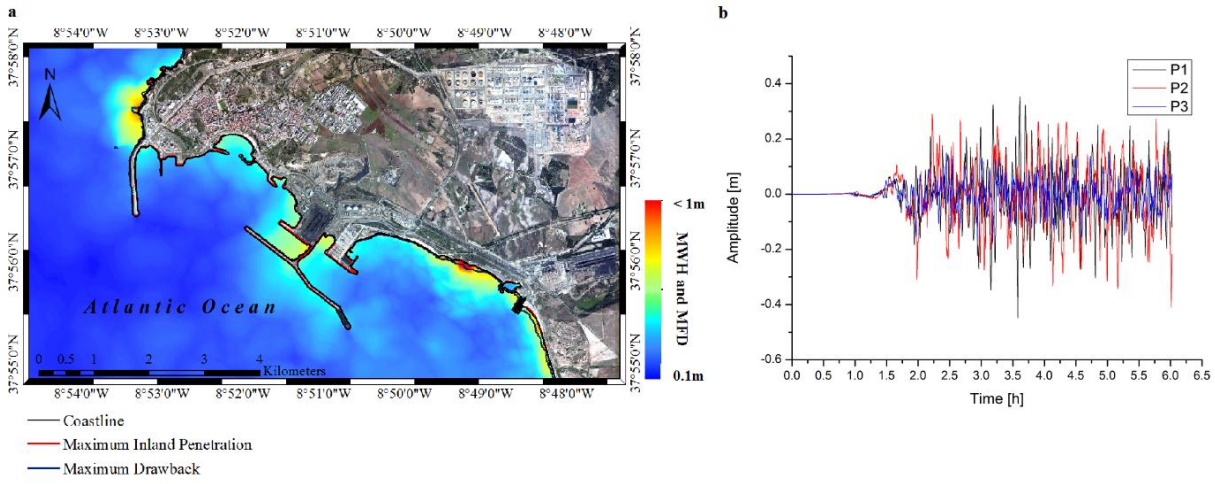

Figure 5. (a) Results MWH, MFD, MDB, MIA and MIP for the Gloria scenario at MSL: MWH and MFD are presented by the colour bar offshore and on land respectively. Offshore and land are separated by the coastline (black line). MDB is indicated by the blue line. The MIA is given between the coastline and the MIP (red line). (b) synthetic waveform for 6h propagation time at 3 chosen points (cf. Fig. 1) for the Gloria scenario.

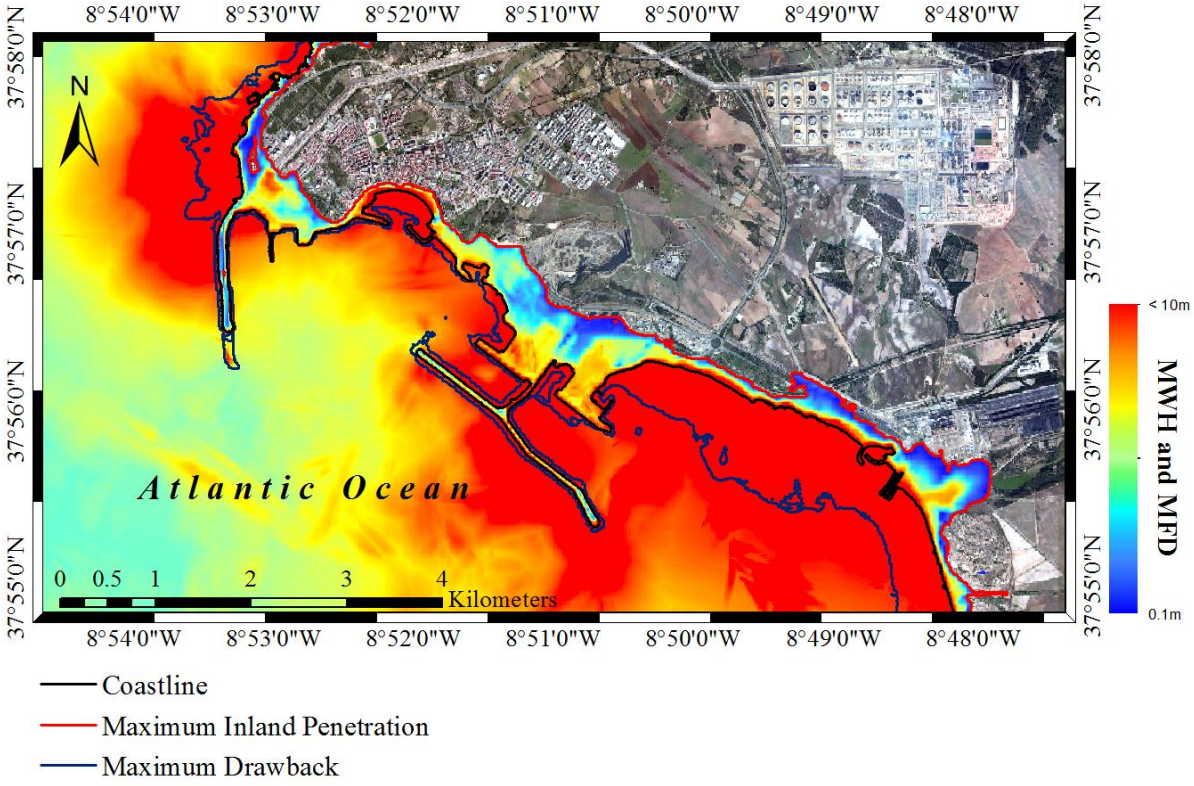

Figure 6. MWH, MFD, MDB, MIA and MIP for the aggregate scenario considering all stages of the tide. MWH offshore and MFD on land are presented by the colour bar. MDB is indicated by the thick dark blue line. The MIA is given between the coastline (black line) and the MIP (red line).

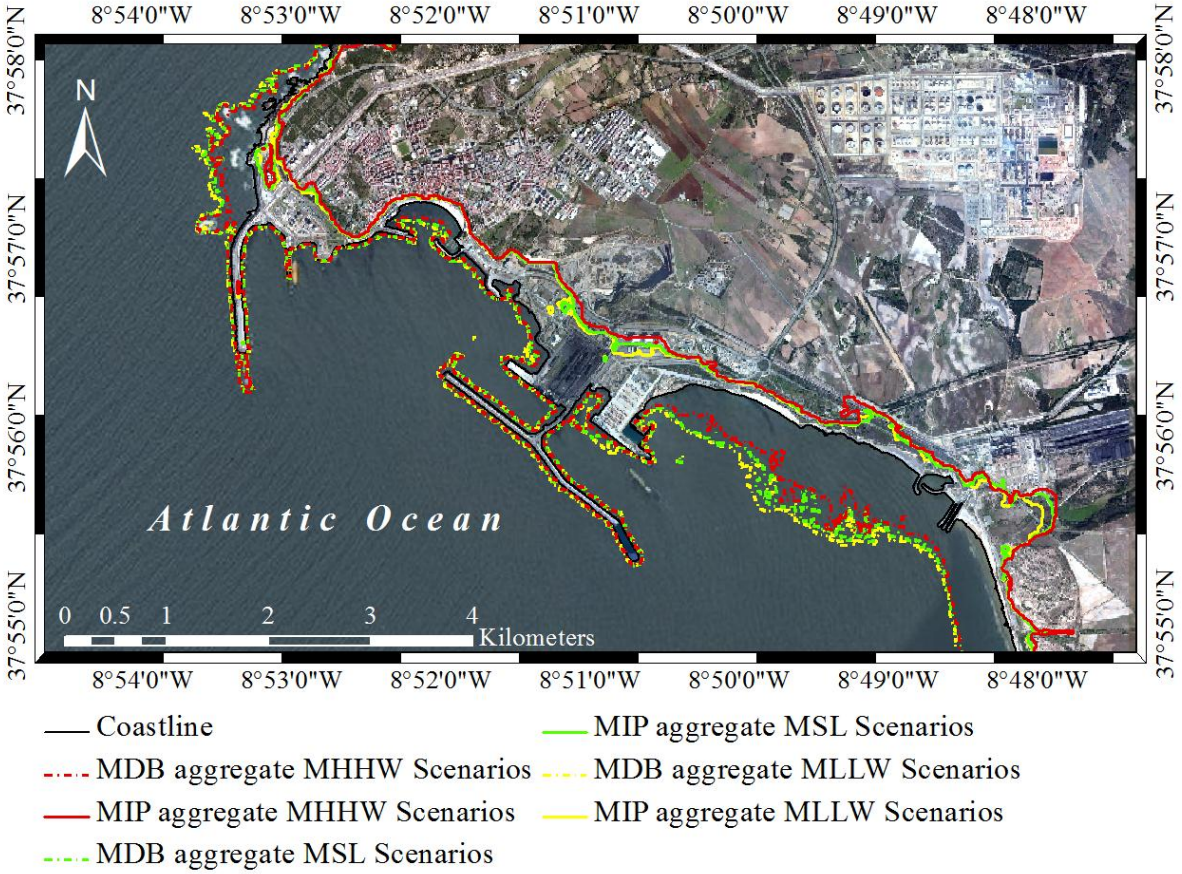

1

2

3 Figure 7. MDB and MIP limits for the stages MLLW, MSL and MHHW of the tide.

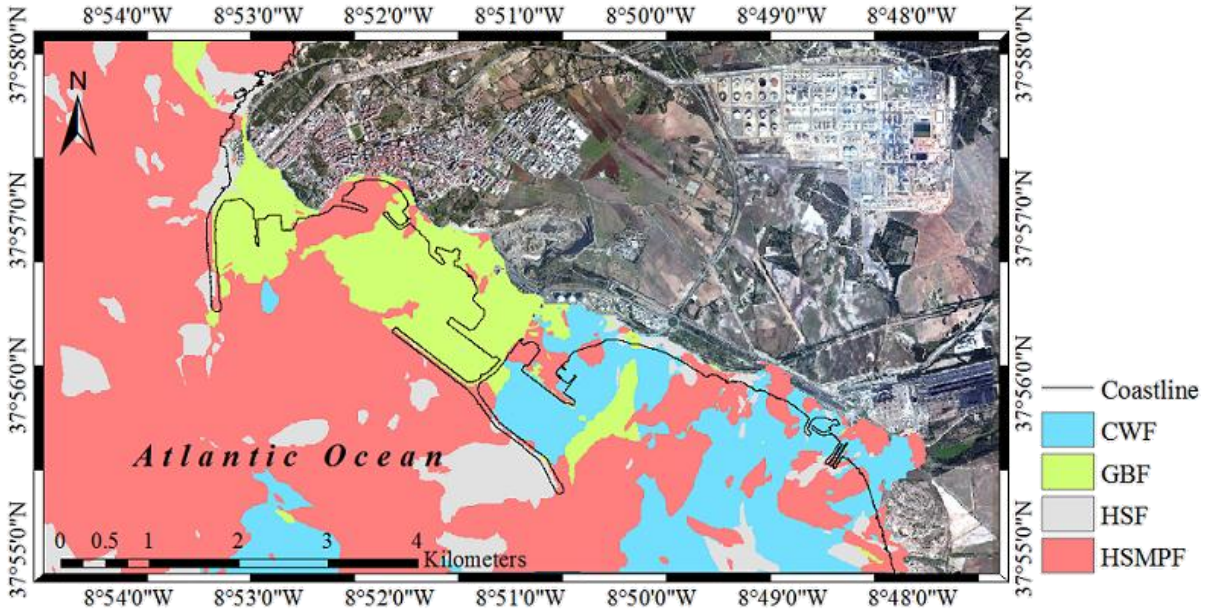

Figure 8. Contribution of individual scenarios considering MWH and MFD to the aggregate model at MSL.